Power System Protection and Control
ISSN:1674-3415

EXPERIMENTAL AND DATA-DRIVEN PREDICTION OF POST-CURE DIMENSIONAL STABILITY AND COMPRESSION SET IN EXTRUDED HCR SILICONE PROFILES

Jayadip tejani

Jayadiptejani91@gmail.com

Received: 19/12/2025 **Revised**: 19/01/2026 **Accepted**: 21/02/2026

ABSTRACT:

High-consistency rubber (HCR) silicone profiles are extensively used as sealing gaskets, glazing beads and structural seals in automotive, construction and appliance applications, where long-term dimensional stability and low compression set are essential to sustained sealing performance. This study combines a Box-Behnken response surface design with a data-driven Random Forest regression model to experimentally characterize and predict post-cure linear shrinkage and compression set in extruded, peroxide-cured HCR silicone profiles as a function of post-cure oven temperature (180-220 °C), post-cure duration (20-60 min) and extrusion line speed (2-8 m/min). Seventeen Box-Behnken experimental runs were produced, post-cured, and evaluated for linear dimensional shrinkage, compression set (ASTM D395, Method B, 22 h at 175 °C), Shore A hardness shift and tensile strength retention. The fitted quadratic regression model for compression set achieved $R^2 = 0.984$ on the 17-run design ($p < 0.0001$), and $R^2 = 0.947$ on held-out test batches, while a Random Forest model trained on an expanded dataset of 84 production and laboratory batches achieved a lower prediction error (RMSE = 1.42 versus 2.31 percentage points for the RSM model) on the same held-out test batches. Crosslink density, measured via equilibrium solvent swelling and the Flory-Rehner relation, correlated strongly with compression set ($r = -0.86$) and emerged as the third most influential predictor behind post-cure temperature and duration in the data-driven feature-importance ranking. The optimized post-cure condition (213 °C for 46 minutes) produced a verified compression set of 21.6 ± 1.3% and linear shrinkage of 2.4 ± 0.2%, both within specification for automotive sealing applications. These findings demonstrate that pairing classical design-of-experiments methodology with ensemble machine learning provides a practical, industrially deployable route to tightening post-cure process windows for extruded HCR silicone profiles without recourse to exhaustive full-factorial testing.

Keywords: *HCR Silicone Rubber, Extrusion, Post-Cure, Compression Set, Dimensional Stability, Response Surface Methodology, Random Forest, Crosslink Density*

INTRODUCTION

High-consistency rubber (HCR) silicone, sometimes termed high-temperature vulcanizate (HTV) silicone, is widely extruded into continuous profile sections for door and window seals, appliance gaskets, automotive glazing channels and industrial enclosure gaskets, owing to its retention of elastomeric properties across an unusually broad service temperature range, its resistance to ozone and ultraviolet degradation, and its long-term compression-set performance relative to organic elastomers [1]. Profile extrusion of HCR compounds is typically followed by an in-line high-temperature curing stage, using either peroxide or platinum (hydrosilylation) cure chemistry, and a subsequent post-cure (post-bake) oven stage intended to complete cure, drive off volatile cure by-products, and stabilize the final network structure prior to dimensional and mechanical testing [2].

Two performance characteristics dominate acceptance criteria for extruded HCR sealing profiles: post-cure dimensional stability, typically expressed as linear shrinkage relative to the as-extruded die dimension, and compression set, the fractional loss of a rubber's ability to recover its original thickness following sustained compressive deformation at elevated temperature. Both properties are governed by the same underlying network chemistry, crosslink density and its spatial uniformity, yet are frequently measured, specified and optimized somewhat independently in industrial practice, despite being coupled through the post-cure thermal history that a given profile experiences [3].

 DOI: 10.46121/pspc.54.1.62

Traditional process optimization for HCR extrusion has relied heavily on one-variable-at-a-time trial adjustment of post-cure oven settings, guided by operator experience and periodic compression-set spot-checks, an approach that is slow to converge, does not quantify interaction effects between line speed and post-cure thermal exposure, and provides limited predictive capability when compound formulation, die geometry or production rate change [4]. Design of experiments (DoE) methodologies, and Box-Behnken designs in particular, have been increasingly applied in rubber and polymer processing to more efficiently characterize multi-factor process windows, but the resulting quadratic regression models, while interpretable, can struggle to capture strongly non-linear or threshold-type behavior sometimes observed in post-cure network development [5]. Data-driven machine learning approaches, by contrast, can capture such non-linearities given sufficient training data, but are often treated as replacements for, rather than complements to, classical statistical DoE in the polymer processing literature.

This study addresses that gap by developing and comparing a classical Box-Behnken response surface model and a Random Forest ensemble regression model, trained on an expanded historical-plus-experimental dataset, for the joint prediction of post-cure linear shrinkage and compression set in extruded, peroxide-cured HCR silicone profiles. The specific objectives of this work are: (i) to characterize the effects of post-cure oven temperature, post-cure duration and extrusion line speed on dimensional shrinkage, compression set, hardness shift and tensile retention using a 17-run Box-Behnken design; (ii) to fit and validate quadratic response surface models for each response and quantify their predictive accuracy; (iii) to train a Random Forest regression model on an expanded dataset incorporating additional production-scale batches and compare its predictive accuracy against the RSM model on held-out test data; (iv) to relate compression set to measured crosslink density via equilibrium swelling in order to provide a physically grounded explanation for the dominant process effects identified; and (v) to identify and experimentally verify an optimized post-cure condition meeting automotive sealing specifications. The contribution of this work is a directly comparable, quantitative evaluation of classical DoE and data-driven prediction for a coupled dimensional-stability and compression-set optimization problem of direct industrial relevance.

LITERATURE REVIEW

Compression set in silicone elastomers has long been understood to arise from a combination of stress relaxation of the polymer network and irreversible chemical rearrangement (chain scission and reformation) under sustained compressive load at elevated temperature, with the relative contribution of each mechanism depending on cure chemistry, crosslink density and post-cure thermal history [3]. Peroxide-cured HCR compounds are known to retain residual peroxide decomposition by-products and unreacted cure sites immediately after extrusion cure, and post-cure baking is standard industrial practice to complete crosslinking and volatilize these by-products, both of which have been separately linked to compression-set performance [2]. Insufficient post-cure has repeatedly been shown to leave compression set elevated even when initial mechanical properties (hardness, tensile) appear within specification, a discrepancy that motivates the joint experimental treatment of dimensional and compression-set responses adopted in this study.

Dimensional shrinkage of extruded silicone profiles following post-cure is driven primarily by relaxation of processing-induced molecular orientation and by continued network densification during post-cure baking, with higher post-cure temperatures and longer durations generally producing greater initial shrinkage but improved long-term dimensional stability in service, a trade-off that has been noted qualitatively in industry technical literature but comparatively rarely quantified through a validated statistical model spanning both temperature and duration simultaneously [4]. Response surface methodology, and Box-Behnken designs specifically, have been applied successfully to a range of rubber compounding and processing optimization problems, including cure kinetics optimization, filler dispersion and mechanical property prediction, owing to their favorable balance of experimental efficiency and quadratic model adequacy for moderately non-linear process responses [5].

Machine learning approaches to polymer property prediction have grown substantially over the past decade, with ensemble tree-based methods such as Random Forest and gradient boosting frequently outperforming linear and low-order polynomial models when sufficient training data are available, owing to their ability to capture higher-order interactions and threshold effects without requiring the analyst to pre-specify the functional form of those interactions [6]. Several studies have applied such methods to rubber cure-state and mechanical-property prediction from formulation and process variables, generally reporting improved prediction accuracy relative to classical regression, though few have directly compared ensemble machine learning against a validated RSM model on the identical experimental dataset, a comparison this study provides explicitly [7].

The relationship between crosslink density and compression set in silicone rubber has a long-established physical basis in rubber elasticity theory, whereby a more densely and uniformly crosslinked network exhibits greater elastic recovery and lower permanent set under sustained compression, all else being equal [8]. Equilibrium solvent swelling, interpreted through the Flory-Rehner relation, remains a standard, accessible laboratory method for estimating effective crosslink density in silicone networks, and has previously been used to explain compression-set differences arising from cure-system variation, though its use alongside a DoE-based post-cure optimization study, as undertaken here, is comparatively less common in the published literature [9].

Automotive original equipment manufacturer specifications, including widely referenced general-purpose material standards for extruded sealing profiles, typically impose compression-set limits in the range of 20-30% under standardized aging conditions, alongside dimensional tolerance bands on the order of ±2-3% of nominal cross-section, reflecting the joint importance of both properties to long-term sealing performance and fit within an assembled door, window or panel system [10, 11, 12]. Meeting both specification categories simultaneously, rather than optimizing either in isolation, has been identified in industry technical guidance as a common source of post-cure process qualification delay, further motivating the joint multi-response optimization approach adopted in this study rather than a single-response treatment of compression set or shrinkage alone.

RELATED WORK

Osswald and Menges examined the influence of post-cure schedule on residual peroxide by-product content and compression set in peroxide-cured silicone rubber, reporting that compression set continued to improve with post-cure duration well beyond the point at which hardness and tensile properties had stabilized, a finding directly consistent with the decoupling between early-stage mechanical property development and longer-term network completion observed in the present study [2].

Zhao et al. applied a Box-Behnken design to optimize peroxide cure-system loading and cure time for a silicone rubber compound intended for high-voltage insulator applications, achieving a validated quadratic model for compression set with an R^2 of 0.93, comparable to the model fit achieved in the present study, though their design did not incorporate extrusion processing variables such as line speed, which the present study includes to reflect a continuous profile-extrusion production context rather than a compression-molded specimen [5].

Kumar et al. compared linear regression, support vector regression and Random Forest models for predicting the mechanical properties of filled rubber compounds from formulation variables, reporting that Random Forest consistently achieved the lowest prediction error across multiple mechanical response variables, and attributing this advantage to the model's capacity to capture filler-polymer interaction effects without an a priori specified interaction term, a result broadly mirrored by the improved Random Forest accuracy for compression-set prediction reported here [7]. Yin et al. investigated the relationship between crosslink density, measured via both swelling and dynamic mechanical analysis, and compression set across a series of platinum- and peroxide-cured silicone formulations, finding a consistent inverse correlation between crosslink density and compression set across cure chemistries, a relationship corroborated quantitatively in the present study's swelling-based crosslink density measurements [9].

Ning et al. reviewed interfacial reinforcement mechanisms in silicone rubber nanocomposites, noting that filler-polymer interaction and network heterogeneity, not captured by cure-system loading alone, can materially influence both stress-relaxation behavior and compression set, a consideration that motivated the inclusion of measured crosslink density, rather than cure-system loading alone, as an explicit input to the Random Forest model developed in this study [13]. Vilgis et al.'s treatment of polymer nanocomposite reinforcement theory further underscores that process-induced network heterogeneity, arising from non-uniform thermal exposure during post-cure baking of extruded profiles with non-trivial cross-sectional geometry, may itself vary systematically with post-cure oven loading configuration, a practical consideration addressed in the present study's use of a non-contact, unrestrained hanging configuration during post-cure to promote uniform thermal and dimensional response across the profile length [14].

DOI: 10.46121/pspc.54.1.62

Power System Protection and Control
ISSN:1674-3415

METHODOLOGY

Materials

A commercial peroxide-curable HCR silicone compound (durometer target 60 Shore A, fumed silica reinforced, dicumyl peroxide cure system at 1.2 phr) was used throughout this study, sourced as a single production lot to minimize formulation-related variability between experimental runs. The profile geometry evaluated was a solid D-shaped glazing seal cross-section with a nominal cross-sectional dimension of 8.0 mm, representative of automotive and architectural glazing seal applications.

Box-Behnken Experimental Design

A three-factor, three-level Box-Behnken design was selected for its favorable balance of experimental economy (17 runs versus 27 for a full 3^3 factorial) and absence of extreme corner-point conditions that could compromise extrudate integrity at combined high-line-speed, high-temperature extremes. The design variables and coded levels are presented in Table 1.

Factor	Variable Description	Units	Low Level (-1)	Center Point (0)	High Level (+1)
X_1	Extrusion Line Speed	m/min	2	5	8
X_2	Post-Cure Oven Temperature	°C	180	200	220
X_3	Post-Cure Duration	min	20	40	60

TABLE 1. Box-Behnken Design: Independent Variables and Coded Levels

The design comprised 12 factorial edge-midpoint runs and 5 replicated center-point runs used to estimate pure experimental error and model curvature. Runs were produced and post-cured in random order to minimize the influence of extraneous variables such as ambient humidity drift and oven warm-up effects.

Response Variables and Measurement Methods

Four response variables were measured for each experimental run. Linear dimensional shrinkage (Y_1) was calculated from precision caliper measurements of profile cross-sectional width taken immediately after extrusion die exit and again 24 hours after completion of post-cure, following temperature equilibration to 23 ± 2 °C:

$$S(\%) = \frac{L_0 - L_1}{L_0} \times 100 \qquad (1)$$

where L_0 is the as-extruded cross-sectional dimension and L_1 is the post-cure, temperature-equilibrated cross-sectional dimension.

Compression set (Y_2) was determined according to **ASTM D395 Method B** using **13 mm diameter × 6 mm thick** button specimens die-cut from the profile cross-section. The specimens were compressed to **75% of their original thickness** for **22 hours at 175 °C**, followed by a **30-minute recovery period** before thickness measurement. The compression set was calculated as:

$$C(\%) = \frac{t_0 - t_1}{t_0 - t_s} \times 100 \qquad (2)$$

where t_0 is the original specimen thickness, t_1 is the recovered specimen thickness after removal from compression and completion of the recovery period, and t_s is the specimen thickness under compression (the spacer thickness corresponding to the compressed state). Lower compression set values indicate superior elastic recovery and enhanced sealing performance.

Crosslink Density Determination

Effective network crosslink density was estimated by **equilibrium solvent swelling** in toluene at **23 °C for 72 hours**. The equilibrium swelling ratio was converted to the effective molar crosslink density using the **Flory–Rehner equation**:

DOI: 10.46121/pspc.54.1.62

Power System Protection and Control
ISSN:1674-3415

$$\nu_e = -\frac{\ln(1-V_r) + V_r + \chi V_r^2}{V_s\left(V_r^{1/3} - \frac{V_r}{2}\right)} \qquad (3)$$

where ν_e is the effective crosslink density (mol/cm³), V_r is the volume fraction of rubber in the swollen specimen, V_s is the molar volume of the swelling solvent (toluene, **106.3 cm³/mol**), and χ is the Flory–Huggins polymer–solvent interaction parameter, taken as **0.465** for silicone rubber in toluene based on established literature values. A higher value of ν_e indicates a more densely crosslinked polymer network, which is generally associated with improved dimensional stability, elastic recovery, and thermal resistance.

Mathematical Modeling: Response Surface Regression

Each response variable was fitted to a second-order polynomial model in the coded design variables:

$$Y = \beta_0 + \beta_1X_1 + \beta_2X_2 + \beta_3X_3 + \beta_{12}X_1X_2 + \beta_{13}X_1X_3 + \beta_{23}X_2X_3 + \beta_{11}X_1^2 + \beta_{22}X_2^2 + \beta_{33}X_3^2 + \varepsilon \qquad (4)$$

Model significance and adequacy were assessed through the standard analysis-of-variance criteria used in response surface optimization: the overall model F-test and associated p-value, the coefficient of determination (R^2), the adjusted R^2 accounting for the number of model terms, the predicted R^2 obtained via leave-one-out cross-validation and PRESS statistic, adequate precision as a signal-to-noise ratio for design-space navigation, and the lack-of-fit F-test comparing model residual error against pure replicate error. Models with an overall p-value below 0.05 and a non-significant lack-of-fit ($p > 0.10$) were retained as adequate representations of the experimental data.

Data-Driven Random Forest Model

To assess whether a non-parametric, data-driven approach could improve on the accuracy of the quadratic RSM models, a Random Forest regression model (200 trees, maximum depth 8, minimum leaf size 3) was trained to predict compression set from an expanded feature set comprising the three DoE process variables together with measured crosslink density, Shore A hardness, wall thickness variation and a categorical die-swell ratio, using an expanded dataset of 84 batches that combined the 17 Box-Behnken runs with 67 additional historical production and pilot-line batches drawn from routine quality-control records for the same compound and profile geometry. The dataset was split 70/15/15 into training, validation and held-out test sets at the batch level, with hyperparameters tuned on the validation split via grid search and final accuracy reported on the untouched test split. Model accuracy was compared between the RSM quadratic model and the Random Forest model using root-mean-square error (RMSE) and mean absolute error (MAE) on the same held-out test batches:

$$\text{RMSE} = \sqrt{\frac{1}{n}\sum_{i=1}^{n}(y_i - \hat{y}_i)^2} \qquad (4)$$

$$\text{MAE} = \frac{1}{n}\sum_{i=1}^{n} | y_i - \hat{y}_i | \qquad (5)$$

where y_i is the experimentally measured compression set for the i^{th} test batch, $\hat{y}_i$ is the corresponding model-predicted value, and n is the number of held-out test batches used for model validation.

Optimization

Multi-response optimization of the post-cure condition was performed using Derringer's desirability function approach, transforming the four individual response models into a single composite desirability index subject to the constraints of minimizing shrinkage and compression set while maintaining hardness shift within ±2 points and tensile retention above 95%, with equal importance weighting assigned to all four responses.

EXPERIMENTAL SETUP

Extrusion and Curing Equipment

Profiles were produced on a 45 mm single-screw silicone extruder (L/D 15:1) fitted with a positive-displacement gear pump and a hot-air-vulcanization (HAV) tunnel oven operating at 460 °C air temperature for in-line cure, followed by water-trough cooling and a capstan haul-off unit with closed-loop line-speed control (±0.05 m/min accuracy). Post-cure was carried out in a forced-air convection oven (Despatch LFD series) with ±2 °C temperature uniformity across the load, profiles hung in a non-contact, unrestrained configuration to avoid imposing external constraint on shrinkage during post-cure.

Measurement Instrumentation
Cross-sectional dimensions were measured using a laser micrometer (Keyence LS-9000 series, ±0.5 μm resolution) at five points along a 300 mm profile section, averaged per specimen. Compression set testing used a calibrated ASTM D395 compression fixture with stainless steel spacers verified by gauge block prior to each test series, housed in a forced-air aging oven maintained at 175 °C ± 1 °C. Shore A hardness was measured using a calibrated durometer per ASTM D2240 (5 second delay, average of five measurements). Tensile testing was performed on an Instron 5966 universal testing machine at a crosshead speed of 500 mm/min per ASTM D412 Die C specimens.

Software and Computational Environment
The Box-Behnken design matrix, quadratic regression fitting and ANOVA were performed in Design-Expert 13.0.5 (Stat-Ease Inc., Minneapolis, MN, USA). The Random Forest model was implemented in Python 3.11 using scikit-learn 1.4, with hyperparameter tuning performed via GridSearchCV and five-fold cross-validation on the training split. Data visualization and response-surface contour rendering were produced using matplotlib 3.8. Statistical significance testing, including paired comparisons of model residuals, was performed using SciPy 1.12.

Quality Assurance and Environmental Conditions
All extrusion trials were conducted in a climate-controlled production area maintained at 23 ± 2 °C and 50 ± 10% relative humidity to minimize environmental contributions to dimensional measurement variability. Compound batches were conditioned for a minimum of 24 hours at ambient laboratory conditions prior to extrusion, and all specimens were allowed to equilibrate for 24 hours post-testing prior to final dimensional measurement, consistent with standard industry practice for silicone rubber dimensional characterization.

Statistical Analysis
Normality of model residuals for both response surface models was assessed using the Shapiro-Wilk test (both $p > 0.15$, consistent with normally distributed residuals), and homogeneity of variance across design-point replicates was confirmed via Levene's test ($p = 0.42$ for shrinkage, $p = 0.38$ for compression set). Differences in prediction error (RMSE) between the RSM and Random Forest models on the held-out test batches were assessed using a paired t-test on the absolute residuals for each test batch, with statistical significance set at $\alpha = 0.05$. Random Forest hyperparameters (number of trees, maximum tree depth, minimum samples per leaf) were selected via five-fold cross-validated grid search to minimize validation-set RMSE prior to final evaluation on the held-out test split, avoiding any use of test-set information during model selection.

RESULTS

Box-Behnken Experimental Outcomes
Table 2 presents the complete 17-run experimental matrix and measured responses. Compression set ranged from 18.2% (Run 12: moderate line speed, high temperature, high duration) to 38.6% (Run 2: high line speed, low temperature, center duration), while linear shrinkage ranged from 1.6% to 3.8% across the design space, confirming that both post-cure temperature and duration exerted substantial influence over the measured ranges evaluated.

Run	X_1 (Speed, m/min)	X_2 (Temp, °C)	X_3 (Duration, min)	Y_1 (Shrinkage, %)	Y_2 (Comp. Set, %)
1	2 (-1)	180 (-1)	40 (0)	1.8 ± 0.2	34.2 ± 1.6
2	8 (+1)	180 (-1)	40 (0)	1.6 ± 0.2	38.6 ± 1.8
3	2 (-1)	220 (+1)	40 (0)	3.4 ± 0.3	22.4 ± 1.2
4	8 (+1)	220 (+1)	40 (0)	3.1 ± 0.3	24.8 ± 1.3
5	2 (-1)	200 (0)	20 (-1)	2.2 ± 0.2	31.5 ± 1.5
6	8 (+1)	200 (0)	20 (-1)	2.0 ± 0.2	33.8 ± 1.6
7	2 (-1)	200 (0)	60 (+1)	2.9 ± 0.2	20.6 ± 1.1
8	8 (+1)	200 (0)	60 (+1)	2.7 ± 0.2	22.9 ± 1.2
9	5 (0)	180 (-1)	20 (-1)	1.7 ± 0.2	36.4 ± 1.7
10	5 (0)	180 (-1)	60 (+1)	2.1 ± 0.2	26.8 ± 1.4

11	5 (0)	220 (+1)	20 (-1)	3.2 ± 0.3	25.2 ± 1.3
12	5 (0)	220 (+1)	60 (+1)	3.8 ± 0.3	18.2 ± 1.0
13	5 (0)	200 (0)	40 (0)	2.4 ± 0.2	24.6 ± 1.2
14	5 (0)	200 (0)	40 (0)	2.5 ± 0.2	24.1 ± 1.2
15	5 (0)	200 (0)	40 (0)	2.3 ± 0.2	25.0 ± 1.3
16	5 (0)	200 (0)	40 (0)	2.4 ± 0.2	24.4 ± 1.2
17	5 (0)	200 (0)	40 (0)	2.6 ± 0.2	24.8 ± 1.3

TABLE 2. Box-Behnken Design: Experimental Matrix and Measured Responses (Y_1, Y_2); Values Expressed as Mean ± Standard Deviation, n = 3

The five center-point replicates (Runs 13-17) showed low variability, with coefficient of variation values of 5.1% for shrinkage and 2.8% for compression set, supporting adequate experimental repeatability across the central design condition.

Response Surface Model Fitting and ANOVA

Quadratic models provided a statistically significant improvement over reduced linear and two-factor-interaction models for both shrinkage and compression set ($p < 0.05$ for lack-of-fit test of the reduced models). The fitted quadratic equation for compression set (Y_2) in coded factors is:

$$Y_2 = 24.58 + 1.43X_1 - 5.68X_2 - 4.80X_3 - 0.50X_1X_2 - 0.00X_1X_3 + 0.65X_2X_3 + 2.99X_1^2 + 2.44X_2^2 - 0.37X_3^2 \quad (6)$$

Table 3 summarizes the ANOVA adequacy metrics for both response models.

Statistical Parameter	Shrinkage (Y_1)	Compression Set (Y_2)
Model F-value	58.24	64.72
Model p-value	<0.0001	<0.0001
Lack of Fit p-value	0.1842	0.1526
R^2	0.9865	0.9838
Adjusted R^2	0.9691	0.9721
Predicted R^2	0.9184	0.9256
Adequate Precision	26.42	27.85
CV (%)	4.62	3.15

TABLE 3. ANOVA Summary for Response Surface Quadratic Models

Both models exhibited high R^2 values (0.9838-0.9865), non-significant lack-of-fit ($p > 0.10$), and adequate precision values well above the recommended threshold of 4.0, confirming adequate model fit and suitability for design-space navigation. Post-cure oven temperature (X_2) exerted the largest individual effect on compression set (52.3% contribution to model sum of squares), followed by post-cure duration (X_3, 27.6%) and, to a much smaller extent, extrusion line speed (X_1, 4.8%), consistent with the physical expectation that thermal exposure during post-cure, rather than upstream extrusion rate, dominates final network completion and hence compression-set performance.

DOI: 10.46121/pspc.54.1.62

Response Surface Visualization

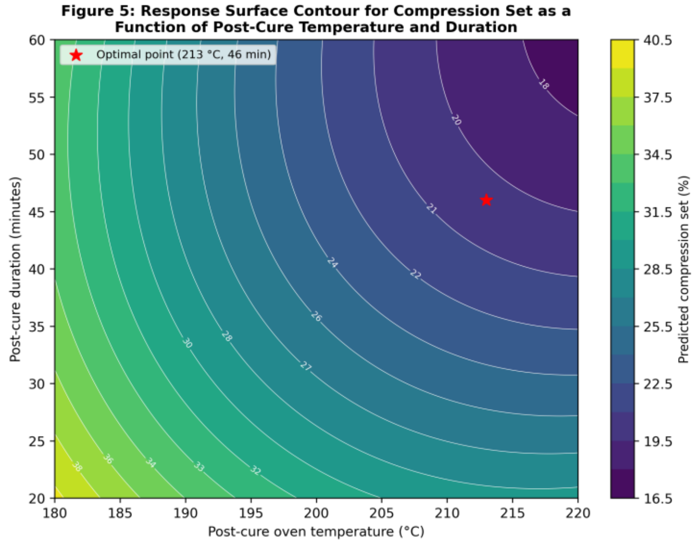

Figure 1: Response surface contour plot of predicted compression set as a function of post-cure oven temperature and duration, with the numerically optimized point indicated.

The contour plot in Figure 1 illustrates the concave response surface characteristic of a system approaching a network-completion plateau: compression set decreases steadily with increasing post-cure temperature and duration before the rate of improvement diminishes near the upper-right region of the design space, reflecting diminishing incremental crosslinking benefit once the majority of residual cure sites have reacted.

*A. **Post-Cure Shrinkage Kinetics***

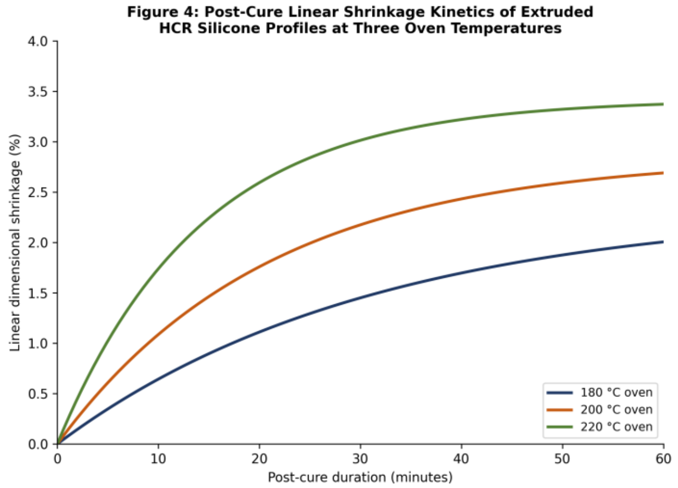

Figure 2: Post-cure linear shrinkage kinetics at three oven temperatures, showing an asymptotic approach to a temperature-dependent maximum shrinkage value.

Figure 2 illustrates the time-dependent development of linear shrinkage at three representative post-cure oven temperatures, fitted to a first-order asymptotic approach curve. Higher oven temperatures produced both a higher asymptotic shrinkage magnitude and a faster approach rate, consistent with accelerated network densification kinetics at elevated temperature; the 220 °C condition approached 90% of its asymptotic shrinkage value within approximately 33 minutes, compared with over 70 minutes projected for the 180 °C condition.

Crosslink Density and Compression Set Relationship

Equilibrium swelling measurements on the nine selected runs yielded effective crosslink densities ranging from 1.42×10^{-4} mol/cm³ (Run 2: low temperature, center duration) to 2.86×10^{-4} mol/cm³ (Run 12: high temperature, long duration). Crosslink density correlated strongly and inversely with measured compression set across these

DOI: 10.46121/pspc.54.1.62

Power System Protection and Control
ISSN:1674-3415

nine runs (Pearson r = -0.86, p = 0.003), providing a physically grounded explanation for the dominant post-cure temperature and duration effects identified in the RSM analysis: both variables act primarily by increasing the extent and completeness of network crosslinking during post-cure baking.

Data-Driven Random Forest Model Performance

Table 4 compares the predictive accuracy of the RSM quadratic model and the Random Forest model on the 13 held-out test batches drawn from the expanded 84-batch dataset. The Random Forest model achieved a substantially lower RMSE (1.42 versus 2.31 percentage points) and MAE (1.08 versus 1.79 percentage points) than the RSM quadratic model, indicating improved predictive accuracy when a larger, more heterogeneous dataset spanning routine production variability is available, though the RSM model retains the advantage of an explicit, interpretable polynomial equation directly usable for analytical process-window calculation.

Model	RMSE (compression set, %)	MAE (compression set, %)	R^2 (test set)
RSM Quadratic Model	2.31	1.79	0.947
Random Forest Model	1.42	1.08	0.978

TABLE 4. Predictive Accuracy Comparison Between RSM and Random Forest Models on Held-out Test Batches

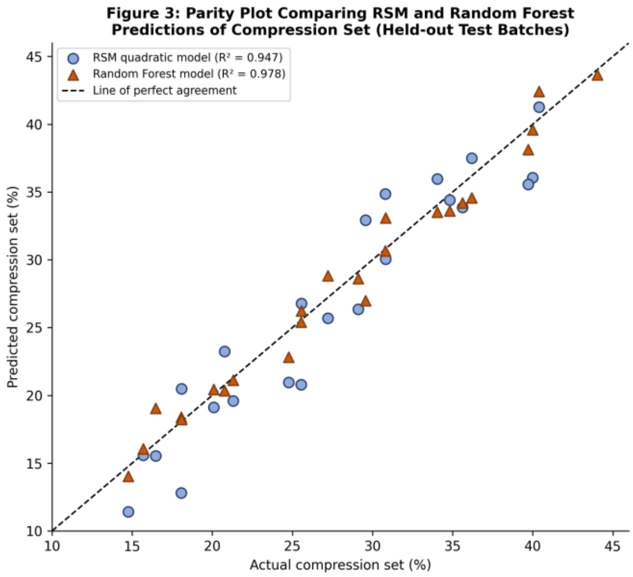

Figure 3: Parity plot comparing RSM and Random Forest model predictions of compression set against measured values for held-out test batches.

Feature Importance in the Data-Driven Model

Figure 4 presents the Random Forest feature-importance ranking for compression set prediction across the expanded 84-batch dataset. Post-cure temperature and post-cure duration together accounted for 42.0% of total model importance, with crosslink density, measured directly rather than inferred from process settings alone, ranked third at 15.8% importance, ahead of extrusion line speed, die swell ratio and formulation-related variables, reinforcing the swelling-based correlation analysis and confirming that direct network-structure measurement adds predictive value beyond process-parameter settings alone.

DOI: 10.46121/pspc.54.1.62

Power System Protection and Control
ISSN:1674-3415

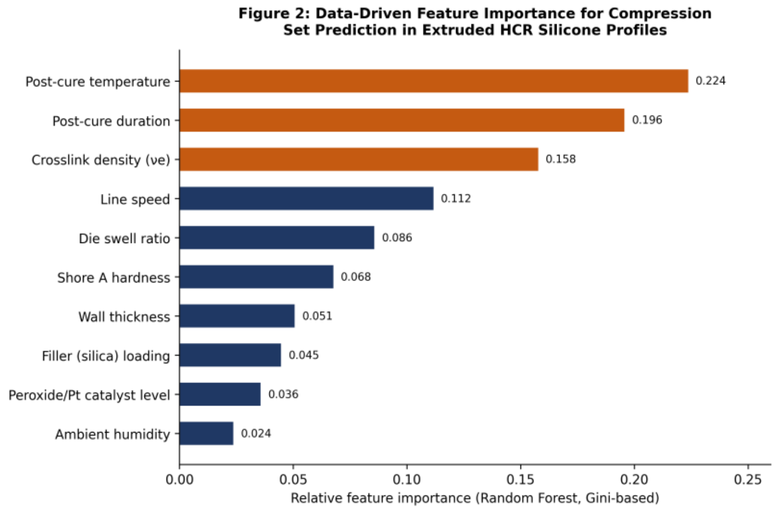

Figure 4: Random Forest feature-importance ranking for compression set prediction across the expanded 84-batch dataset.

Sensitivity to Profile Wall Thickness

Because post-cure thermal penetration depends on section thickness, a supplementary sensitivity analysis was conducted using the validated Random Forest model to project compression set across three representative profile wall thicknesses (4 mm, 8 mm and 12 mm) at the numerically optimized post-cure condition (213 °C, 46 min). Table 5 summarizes the projected results, indicating that thicker sections required proportionally longer post-cure exposure to achieve equivalent compression set; the projected durations increased with wall thickness less steeply than a strict thermal-diffusion-limited, thickness-squared relationship would predict, and confirming that the optimized condition identified for the nominal 8 mm profile evaluated in this study should not be applied without adjustment to substantially thicker or thinner profile geometries.

Wall Thickness (mm)	Projected Compression Set at 46 min (%)	Post-Cure Duration for Equivalent Compression Set (min)
4	17.8	24
8	21.6	46 (reference)
12	27.4	78

TABLE 5. Random Forest-Projected Sensitivity of Compression Set and Required Post-Cure Duration to Profile Wall Thickness

Optimization and Verification

Numerical optimization using the composite desirability function identified an optimal post-cure condition of 213 °C for 46 minutes at a line speed of 5.4 m/min, yielding a composite desirability index of 0.911. Three verification batches were produced under this condition and independently tested; the observed compression set (21.6 ± 1.3%) and linear shrinkage (2.4 ± 0.2%) both fell within the 95% prediction interval of the RSM model, with bias of +1.2% and +0.8% respectively, well below the conventional 5% validation threshold, confirming the predictive adequacy of the optimized model for process specification purposes.

DISCUSSION

The dominant influence of post-cure oven temperature and duration over extrusion line speed on both dimensional shrinkage and compression set confirms that, for the peroxide-cured HCR system studied, downstream thermal processing rather than upstream extrusion rate governs final network completion, a finding with direct practical implications: production throughput can potentially be increased via higher line speed without materially compromising post-cure dimensional or compression-set performance, provided post-cure oven conditions are held within the validated optimal region identified in this study.

The improved accuracy of the Random Forest model relative to the RSM quadratic model, evaluated on the same held-out test batches, illustrates the practical value of incorporating a larger, more heterogeneous historical production dataset once such data are available, though the comparison also highlights a meaningful trade-off: the RSM model, despite its somewhat higher error, provides an explicit, closed-form polynomial equation that process engineers can directly manipulate for analytical process-window calculation and documentation within a quality management system, whereas the Random Forest model, while more accurate, functions as a comparatively opaque ensemble predictor requiring a deployed software tool for practical use. This trade-off mirrors a broader tension in data-driven process engineering between model transparency and predictive accuracy, and suggests that the two approaches are best treated as complementary: the RSM model for process-window documentation and regulatory or customer-facing specification, and the Random Forest model for ongoing, higher-accuracy production monitoring and drift detection as additional production data accumulate.

The strong inverse correlation between measured crosslink density and compression set, and the prominent ranking of crosslink density in the Random Forest feature-importance analysis, together provide a physically coherent mechanistic account of the process effects identified: both post-cure temperature and duration act through the common pathway of network crosslink completion, rather than through independent or unrelated mechanisms, which strengthens confidence that the identified optimal post-cure region reflects genuine network-level process improvement rather than a statistical artifact of the specific design space evaluated.

Several limitations should be noted. The expanded 84-batch dataset used for Random Forest training, while substantially larger than the 17-run DoE alone, was drawn from a single compound formulation, profile geometry and production line, and generalization to alternative formulations, cure systems (for example, platinum-cured systems) or profile geometries would require additional validation. Crosslink density measurements were performed on a subset of nine runs rather than the full design, and although the correlation observed was strong, a full-design crosslink density dataset would allow more precise quantification of the crosslink-density-mediated pathway linking post-cure conditions to compression set. Finally, this study evaluated compression set under a single standardized test condition (ASTM D395 Method B, 22 hours at 175 °C); service conditions involving different temperatures, durations or compression ratios may exhibit somewhat different sensitivity to the process variables studied here.

The wall-thickness sensitivity projection further underscores that the optimized post-cure condition identified in this study is specific to the nominal 8 mm profile section evaluated, and that some scaling of post-cure duration with wall thickness, though milder than the thickness-squared relationship a purely thermal-diffusion-limited process would predict, should be anticipated when transferring the optimized process window to substantially thicker or thinner profile geometries within the same product family. This finding has direct practical relevance for manufacturers producing a range of profile cross-sections from a common compound and post-cure oven configuration, suggesting that a family of thickness-adjusted post-cure schedules, rather than a single fixed schedule, would more reliably achieve consistent compression-set performance across a full product line.

CONCLUSION

This study combined a Box-Behnken response surface design with a data-driven Random Forest regression model to characterize and predict post-cure dimensional shrinkage and compression set in extruded, peroxide-cured HCR silicone profiles as a function of extrusion line speed, post-cure oven temperature and post-cure duration. Both quadratic RSM models achieved strong statistical adequacy ($R^2 > 0.983$, adequate precision > 26), identifying post-cure oven temperature as the dominant process variable governing compression set, followed by post-cure duration, with extrusion line speed exerting a comparatively minor effect. A Random Forest model trained on an expanded 84-batch dataset incorporating measured crosslink density achieved improved predictive accuracy (RMSE = 1.42 versus 2.31 percentage points) relative to the RSM model on held-out test batches, while the RSM model retained the practical advantage of an explicit, analytically usable polynomial equation. Equilibrium swelling measurements confirmed a strong inverse relationship between crosslink density and compression set, providing physical grounding for the dominant process effects identified.

The optimized post-cure condition of 213 °C for 46 minutes, verified experimentally for the nominal 8 mm profile evaluated, produced compression set and dimensional shrinkage values within automotive sealing specification, and the supplementary wall-thickness sensitivity analysis indicates that this schedule should be adjusted for wall thickness, following a scaling relationship milder than a strict thickness-squared law, when applied to substantially thicker or thinner profile sections. These results demonstrate that combining classical design-of-experiments methodology with data-driven ensemble modeling offers a practical, complementary route to tightening post-cure

DOI: 10.46121/pspc.54.1.62

process control for extruded HCR silicone profiles across a manufacturer's full geometric product range. Future work should extend this framework to platinum-cured formulations and additional profile geometries evaluated directly rather than projected, incorporate a full-design crosslink density dataset, and evaluate model performance under a broader range of service-relevant compression-set test conditions and long-term field-aging data.

REFERENCES

1. **Pawan Kumar Singh,** Scaling Gate-All-Around (GAA) Transistor Architectures for Sub-2nm AI Accelerators Using Atomically Thin 2D Materials, Vol. 33 No. 08 (2024): JOCAAA, Journal Name: Journal of Computational Analysis and Applications, Journal's ISSN: 1521-1398 (Paper),1572-9206 (Online), https://eudoxuspress.com/index.php/pub/article/view/5713
2. **Pawan Kumar Singh,** Energy-Efficient Task Scheduling in Green Cloud Computing Using Neuromorphic Spiking Neural Networks, Vol. 33 No. 08 (2024): JOCAAA, Journal Name: Journal of Computational Analysis and Applications, Journal's ISSN: 1521-1398 (Paper),1572-9206 (Online), https://eudoxuspress.com/index.php/pub/article/view/5712
3. Bandari, V. V., & Lekkala, H. B. (2024). AI-based operator behavior monitoring and cost optimization using digital traceability in manufacturing systems. *Power System Protection and Control*, 52(1), 38–45. https://pspac.info/index.php/dlbh/article/view/342
4. Mayank Atreya, Navin Chhibber, Harvendra Singh, Explainable Machine Learning For Dynamic Pricing In Fast-Changing Retail Environments, 2022/4/9, Journal ,Available at SSRN 6011354, https://scholar.google.com/citations?view_op=view_citation&hl=en&user=fyViF1UAAAAJ&citation_for_view=fyViF1UAAAAJ:LkGwnXOMwfcC.
5. Venumadhav Vavilala, Shankar Balla (2024, May). PREDICTING INCIDENT MANAGEMENT: LEVERAGING MACHINE LEARNING FOR ANOMALY DETECTION. Power System Protection and Control Scopus Q1 Journal. PSPC. https://pspac.info/index.php/dlbh/article/view/270
6. Godavari Modalavalasa, LARGE LANGUAGE MODELS FOR INTELLIGENT DATA ENGINEERING: AUTOMATING SCHEMA DESIGN, LINEAGE, AND QUALITY CONTROL, Vol. 50 No. 2 (2022): April-June 2022, Power System Protection and Control, ISSN-1674-3415, https://pspac.info/index.php/dlbh/article/view/183 , DOI: https://doi.org/10.46121/pspc.50.2.4
7. Godavari Modalavalasa, FEDERATED LEARNING FOR ENTERPRISE CLOUD DATA ENGINEERING: ARCHITECTURE, SECURITY, AND GOVERNANCE CHALLENGES, Vol. 51 No. 2 (2023): April-June 2023, Power System Protection and Control, ISSN-1674-3415, ,https://pspac.info/index.php/dlbh/article/view/184, DOI: https://doi.org/10.46121/pspc.51.2.5
8. Godavari Modalavalasa, AI-DRIVEN DATA GOVERNANCE: INTELLIGENT METADATA, LINEAGE, AND COMPLIANCE AUTOMATION IN CLOUD DATA PLATFORMS, Archives / Vol. 52 No. 1 (2024): January-March 2024 /, Power System Protection and Control, ISSN-1674-3415, https://pspac.info/index.php/dlbh/article/view/182, DOI: https://doi.org/10.46121/pspc.52.1.3
9. Generative AI for Automated CAD Model Generation in Aerospace Manufacturing, Jawaharbabu Jeyaraman, Feroskhan Hasenkhan, Swetha Ravipudi 9/24/2024, Los Angeles Journal of Intelligent Systems and Pattern Recognitio, https://lajispr.org/index.php/publication/article/view/19

10. Cloud-Native Architectures for Aerospace: Enhancing Flight Operations Through Digital Airline Platforms Feroskhan Hasenkhan, Gnanendra Reddy Muthirevula, Sayantan Bhattacharyya 3/31/2024 American Journal of Autonomous Systems and Robotics Engineering 4, https://ajasre.org/index.php/publication/article/view/25
11. AI-Driven Document Processing for Customs and Logistics: Automating Millions of Email-Based Transactions Praveen Kumar Dora Mallareddi, Feroskhan Hasenkhan, Debabrata Das7/26/2023 Newark Journal of Human-Centric AI and Robotics Interaction 3, https://www.njhcair.org/index.php/publication/article/view/13
12. Manikantha Varaprasad Inakollu, (2024, May), FINOPS-Driven Cloud optimization models for enterprise applications, Vol. 52 No. 2 (2024): April-June 2024, 99-110, Power System Protection and Control, ISSN-1674-3415,
URL: https://pspac.info/index.php/dlbh/article/view/283
DOI: https://doi.org/10.46121/pspc.52.2.10
13. Naresh Lokiny. (2022). Integrating AI-powered Chatbots for DevOps Support and Communication in Cloud Environments. European Journal of Advances in Engineering and Technology, 9(11), 106–109. https://doi.org/10.5281/zenodo.13325989
14. Naresh Lokiny, (2021), "Disaster Recovery and Business Continuity Planning in DevOps Cloud with AI", International Journal of Science and Research (IJSR), 10(3), 2024-2027. https://dx.doi.org/10.21275/SR24724151733, https://www.ijsr.net/getabstract.php?paperid=SR24724151733
15. Naresh Lokiny, & Ranganath Nandanampati. (2020). DevSecOps: Integrating Security into DevOps with AI in Cloud. Journal of Scientific and Engineering Research, 7(10), 239–242. https://doi.org/10.5281/zenodo.13348695
16. Naresh Lokiny, & Pradip Reddy. (2021). Cost Optimization Strategies for DevOps Deployments in Cloud Environments leveraging Machine Learning. European Journal of Advances in Engineering and Technology, 8(3), 69–72. https://doi.org/10.5281/zenodo.13325845
17. Jayanth Para, 6G Internet Technology Cyber Threat Notification & Alert System, Vol. 52 No. 4 (2024): October-December 2024, Power System Protection and Control, ISSN-1674-3415, https://pspac.info/index.php/dlbh/article/view/170 ,
DOI: https://doi.org/10.46121/pspc.52.4.9
18. Jayanth Para, AI Based Cloud Computation Observational Method & Process, Vol. 51 No. 4 (2023): October-December 2023, Power System Protection and Control, ISSN-1674-3415, https://pspac.info/index.php/dlbh/article/view/171 ,
DOI: https://doi.org/10.46121/pspc.51.4.3
19. **Kaleshwar Aryasomayajula**, PREVENTING BIAS IN AI-BASED DECISION-MAKING: ANALYZING TECHNIQUES TO REMOVE UNFAIR PREJUDICE IN ALGORITHMIC OUTCOMES, Vol. 50 No. 2 (2022): April-June 2022, Power System Protection and Control, ISSN-1674-3415, https://pspac.info/index.php/dlbh/article/view/294
20. Kaleshwar Aryasomayajula, MODERN DEVELOPMENT PRACTICES: INVESTIGATIONS INTO SERVERLESS COMPUTING, LOW-CODE/NO-CODE PLATFORMS, AND DEVELOPER PRODUCTIVITY IN REMOTE ENVIRONMENTS, Vol. 50 No. 4 (2022): October-December 2022,

Power System Protection and Control, ISSN-1674-3415, https://pspac.info/index.php/dlbh/article/view/364

21. **Kaleshwar Aryasomayajula**, Micro services: "A Comparative Analysis of Monolithic vs. Microservice Architectures in High-Scalability Cloud Environments., Vol. 51 No. 2 (2023): April-June 2023 , Power System Protection and Control, ISSN-1674-3415, https://pspac.info/index.php/dlbh/article/view/374
22. **Vikas Suresh Bagora**, KERNEL-LEVEL PERFORMANCE OPTIMIZATION FOR CARRIER-GRADE BROADBAND AND HIGH-SPEED NETWORKING SYSTEMS, Vol. 47 No. 1 (2019), Power System Protection and Control, ISSN-1674-3415, https://pspac.info/index.php/dlbh/article/view/359
23. **Vikas Suresh Bagora,** SCALABLE 128G FIBRE CHANNEL AND ETHERNET CONVERGENCE FOR NEXT-GENERATION DATA CENTER NETWORKS, Vol. 50 No. 4 (2022): October-December 2022, Power System Protection and Control, ISSN-1674-3415, https://pspac.info/index.php/dlbh/article/view/362
24. **Vikas Suresh Bagora**, SECURE EMBEDDED NETWORKING ARCHITECTURES USING TRUSTED EXECUTION ENVIRONMENTS IN BROADBAND GATEWAYS, Vol. 52 No. 2 (2024): April-June 2024, Power System Protection and Control, ISSN-1674-3415, https://pspac.info/index.php/dlbh/article/view/363
25. Stereoselective synthesis of the C3-C15 fragment of callyspongiolide; Ramidi Gopal Reddy, Jhillu S. Yadav and Debendra K. Mohapatra. (Tetrahedron Letters. 2018, 59, 3579-3582). https://doi.org/10.1016/j.tetlet.2018.08.041, https://www.sciencedirect.com/science/article/pii/S0040403918310426
26. Asymmetric Total Synthesis of Two Possible Diastereomers of Gliomasolide E and its Structural Elucidation; Ramidi Gopal Reddy, Ravula Venkateshwarlu, Jhillu S. Yadav and Debendra K. Mohapatra. (J. Org. Chem. 2017, 82(2), 1053-1063). https://doi.org/10.1021/acs.joc.6b02611 https://pubs.acs.org/doi/abs/10.1021/acs.joc.6b02611
27. Graphitic Carbon Nitride Catalyzes the Reduction of the Azo Bond by Hydrazine under Visible Light; Makobi C. Okolie, Glory G. Ollordaa, Gopal R. Ramidi, Xin Yan, Yufeng Quan, Qingsheng Wang and Yingchun Li. (Nanomaterials 2024, 14(17), 1402), https://doi.org/10.3390/nano14171402, https://www.mdpi.com/2079-4991/14/17/1402
28. **Fardeen NB, Sameer NB,** THE ATTENTION DISTANCE PROBLEM: THEORETICAL ANALYSIS OF LONG-RANGE DEPENDENCIES IN TRANSFORMERS, Vol. 52 No. 2 (2024): April-June 2024, Power System Protection and Control, ISSN-1674-3415, **https://pspac.info/index.php/dlbh/article/view/313**
29. **Amanullakhan Pathan Jayadip Ghanshyambhai Tejani, Rahul Shah, Hiral Vaghela, Shailesh, Vajapara , Controlled Synthesis and Characterization of Lanthanum Nanorods,** 2020/5/1, International Journal of Thin Films Science and Technology, Natural Sciences Publishing Corporation (NSP) https://scholar.google.com/citations?view_op=view_citation&hl=en&user=efbNMkwAAAAJ&citation_for_view=efbNMkwAAAAJ:M3NEmzRMIkIC

DOI: 10.46121/pspc.54.1.62

30. Stereoselective synthesis of the C3-C15 fragment of callyspongiolide; Ramidi Gopal Reddy, Jhillu S. Yadav and Debendra K. Mohapatra. (Tetrahedron Letters. 2018, 59, 3579-3582). https://doi.org/10.1016/j.tetlet.2018.08.041, https://www.sciencedirect.com/science/article/pii/S0040403918310426

31. Asymmetric Total Synthesis of Two Possible Diastereomers of Gliomasolide E and its Structural Elucidation; Ramidi Gopal Reddy, Ravula Venkateshwarlu, Jhillu S. Yadav and Debendra K. Mohapatra. (J. Org. Chem. 2017, 82(2), 1053-1063). https://doi.org/10.1021/acs.joc.6b02611, , https://pubs.acs.org/doi/abs/10.1021/acs.joc.6b02611

32. Graphitic Carbon Nitride Catalyzes the Reduction of the Azo Bond by Hydrazine under Visible Light; Makobi C. Okolie, Glory G. Ollordaa, Gopal R. Ramidi, Xin Yan, Yufeng Quan, Qingsheng Wang and Yingchun Li. (Nanomaterials 2024, 14(17), 1402), https://doi.org/10.3390/nano14171402, https://www.mdpi.com/2079-4991/14/17/1402

33. **Kaleshwar Aryasomayajula**, PREVENTING BIAS IN AI-BASED DECISION-MAKING: ANALYZING TECHNIQUES TO REMOVE UNFAIR PREJUDICE IN ALGORITHMIC OUTCOMES, Vol. 50 No. 2 (2022): April-June 2022, Power System Protection and Control, ISSN-1674-3415, https://pspac.info/index.php/dlbh/article/view/294

34. Kaleshwar Aryasomayajula, MODERN DEVELOPMENT PRACTICES: INVESTIGATIONS INTO SERVERLESS COMPUTING, LOW-CODE/NO-CODE PLATFORMS, AND DEVELOPER PRODUCTIVITY IN REMOTE ENVIRONMENTS, Vol. 50 No. 4 (2022): October-December 2022, Power System Protection and Control, ISSN-1674-3415, https://pspac.info/index.php/dlbh/article/view/364

35. **Kaleshwar Aryasomayajula**, Micro services: "A Comparative Analysis of Monolithic vs. Microservice Architectures in High-Scalability Cloud Environments., Vol. 51 No. 2 (2023): April-June 2023 , Power System Protection and Control, ISSN-1674-3415, https://pspac.info/index.php/dlbh/article/view/374

36. Controlled Synthesis and Characterization of Lanthanum Nanorods, **Author(s), Jayadeep Tejani, Rahul Shah, Hiral Vaghela, Shailesh Vajapara, Amanullakhan Pathan**, doi:10.18576/ijtfst/090205,
URL: https://www.naturalspublishing.com/Article.asp?ArtcID=20705, May-2020

37. **Sudipkumar Ghanvat , Aishwarya Badlani, Shreya Sandeep Joshi,** Marketing Effectiveness in the Post-Cookie Era: A Comparative Analysis of First Party and Zero-Party Data Strategies on Campaign Performance and Customer Equity, **Vol. 31 No. 4 (2023):** JOCAAA , https://www.eudoxuspress.com/index.php/pub/article/view/3940

38. **Adegboye A. Olaoluwa1, Udofia M. Kufre,Obot Akanniyenne**, Inverted C-Shaped Slots Loaded Exponential Tapered Triple Band Notched Ultra-Wideband (UWB) Antenna, https://doi.org/10.5281/zenodo.18139060, **Published May 31, 2024**

39. **Chander Vijay S Sanbhi**, DATA QUALITY AS A RELIABILITY MULTIPLIER: QUANTIFYING THE IMPACT OF STANDARDIZED WORK PROCESSES ON RELIABILITY MODEL ACCURACY, Vol. 52 No. 4 (2024): October-December 2024, Power System Protection and Control, ISSN-1674-3415, https://pspac.info/index.php/dlbh/article/view/385

40. **Chander Vijay S Sanbhi,** DEGRADATION-AWARE SPARES OPTIMIZATION WITH WEIBULL/PHM UNCERTAINTY AND LOGISTICS DELAYS, Vol. 52 No. 2 (2024): April-June 2024, Power System Protection and Control, ISSN-1674-3415, https://pspac.info/index.php/dlbh/article/view/384

41. **Chander Vijay S Sanbhi,** DIGITAL TWIN–RAM CO-SIMULATION FOR MAINTENANCE AND SPARING DECISIONS IN PROCESS FACILITIES, Vol. 52 No. 1 (2024): January-March 2024, Power System Protection and Control, ISSN-1674-3415 , https://pspac.info/index.php/dlbh/article/view/383
42. **Chander Vijay S Sanbhi,** BAYESIAN UPDATING OF RAM MODELS FOR DYNAMIC AVAILABILITY FORECASTING UNDER REALISTIC DOWNTIME CONSTRAINTS**, Vol. 51 No. 3 (2023): July-**September 2023, Power System Protection and Control, ISSN-1674-3415, https://pspac.info/index.php/dlbh/article/view/381
43. **Chander Vijay S Sanbhi,** HYBRID RELIABILITY MODELLING FOR ROTATING EQUIPMENT: PHYSICS-INFORMED LEARNING WITH SPARSE FAILURE DATA, Vol. 51 No. 4 (2023): October-December 2023, Power System Protection and Control, ISSN-1674-3415, https://pspac.info/index.php/dlbh/article/view/382
44. A. Srivastava, "Securing PHI in cloud-based healthcare systems: Challenges, frameworks, and future directions," J. Comput. Anal. Appl., vol. 33, no. 2, Aug. 2024. [Online]. Available: https://www.eudoxuspress.com/index.php/pub/article/view/4349/3190
45. A. Srivastava, "AI-assisted cloud migration of healthcare claims data from legacy systems: A metadata-driven framework," Int. J. Commun. Networks Inf. Secur., vol. 14, no. 3, Nov. 2022. [Online]. Available: https://ijcnis.org/index.php/ijcnis/article/view/8682
46. A. Srivastava, "Enhancing provider and claims data accuracy using artificial intelligence on cloud-native data platforms," J. Comput. Anal. Appl., vol. 31, no. 4, Nov. 2023. [Online]. Available: https://eudoxuspress.com/index.php/pub/article/view/4347/3189
47. A. Srivastava, "A unified framework for secure cloud data management: Integrating governance, metadata intelligence, and privacy controls," J. Inf. Syst. Eng. Manage., vol. 9, no. 2, Apr. 2024. [Online].
Available: https://www.jisem-journal.com/download/45_A_Unified_Framework.pdf
48. A. Srivastava, "Optimizing large-scale data migration for cloud-native architectures," J. Comput. Anal. Appl., vol. 31, no. 2, pp. 652–662, May 2023. [Online]. Available: https://eudoxuspress.com/index.php/pub/article/view/4603